



Published in final edited form as:

Proc Conf Inf Sci Syst. 2012 March ; 2012: .

Observability of Neuronal Network Motifs

Andrew J. Whalen^{*,†}, Sean N. Brennan^{*,†}, Timothy D. Sauer[§], and Steven J. Schiff^{*,‡}

Andrew J. Whalen: awhalen@psu.edu; Sean N. Brennan: sbrennan@psu.edu; Timothy D. Sauer: tsauer@gmu.edu; Steven J. Schiff: sshiff@psu.edu

^{*}Center for Neural Engineering, Penn State University, University Park, PA 16802

[†]Department of Mechanical Engineering, Penn State University, University Park, PA 16802

[‡]Department of Engineering Science and Mechanics, Neurosurgery, and Physics, Penn State University, University Park, PA 16802

[§]Department of Mathematical Sciences, George Mason University, Fairfax, VA 22030

Abstract

We quantify observability in small (3 node) neuronal networks as a function of 1) the connection topology and symmetry, 2) the measured nodes, and 3) the nodal dynamics (linear and nonlinear). We find that typical observability metrics for 3 neuron motifs range over several orders of magnitude, depending upon topology, and for motifs containing symmetry the network observability decreases when observing from particularly confounded nodes. Nonlinearities in the nodal equations generally decrease the average network observability and full network information becomes available only in limited regions of the system phase space. Our findings demonstrate that such networks are partially observable, and suggest their potential efficacy in reconstructing network dynamics from limited measurement data. How well such strategies can be used to reconstruct and control network dynamics in experimental settings is a subject for future experimental work.

I. Introduction

An observer model of a natural system has many useful applications in nonlinear dynamics from weather prediction to neuronal systems [1]. A fundamental question that arises when utilizing filters to estimate the future states of a system is how to choose a model and measurement function that faithfully captures the system dynamics and can predict future states [2], [3]. An observer is a model of a system or process that assimilates data from the natural system being modeled. The key concept to employ in a “well designed” observer is observability, which quantifies whether there is sufficient information contained in the measurement to adequately reconstruct the full system dynamics. From the theories of differential embeddings and nonlinear reconstruction we have a nonlinear measure of observability from the so called differential embedding map, comprised of the measurement function and its higher Lie derivatives. The differential embedding map of an observer provides the information contained in a given measurement function and model, which can

be quantified by an observability index [4]. Computed from the Jacobian of the differential embedding map, the observability index is a matrix condition number which quantifies the perturbation sensitivity (closeness to singularity) of the mapping created by the measurement function used to observe the system. Singularities in the map cause observability to decrease and information about the system to be lost.

II. Background

A. Linear Observability

In the early 1960s, Rudolph Kalman introduced the notions of state space decomposition, controllability and observability into the theory of linear systems [5]. From this seminal work comes the classic concept of linear observability for a linear time-invariant (LTI) dynamic system, which defines a ‘yes’ or ‘no’ answer whether a state can be reconstructed from a measurement using the Kalman rank condition check, i.e. $\text{rank}(O) = n$ of the observability matrix O , where n is the dimension of the system (number of state variables).

A dynamic model for a linear system can be represented by

$$\begin{aligned} \dot{\mathbf{x}} &= A\mathbf{x} + B\mathbf{u} \\ y &= C\mathbf{x} \end{aligned} \quad (1)$$

where $\mathbf{x} \in \mathbb{R}^n$ represents the state variable, $\mathbf{u} \in \mathbb{R}^m$ is the external input to the system and $y \in \mathbb{R}^p$ is the output (measurement) function of the state variable. The linear observability matrix is defined as [6]

$$O = \begin{bmatrix} C \\ CA \\ CA^2 \\ \vdots \\ CA^{n-1} \end{bmatrix} \quad (2)$$

The finite limit of the matrix comes from the Cayley-Hamilton theorem [6].

B. Differential Embeddings and Nonlinear Observability

From early work on the nonlinear extensions of observability in the 1970s [7], [8] showed that the observability matrix for nonlinear systems could be expressed using the measurement function and its higher order Lie derivatives with respect to the nonlinear system equations. Again, the core idea is to evaluate a mapping ϕ from the measurements to the states. In particular, Hermann and Krener [7] showed that the space of the measurement function is embedded in \mathbb{R}^p when the mapping from measurement to states is everywhere differentiable and injective by the Whitney Embedding Theorem [9], [10]. In other words, an embedding is a map involving differential structure that does not collapse points or tangent directions [11]. A map ϕ is an embedding when the determinant of the map

Jacobian, $\text{Det} \left(\frac{\partial \phi}{\partial \mathbf{x}} \Big|_{\forall \mathbf{x} \in \mathbb{R}^n} \right)$, is non-vanishing (everywhere differentiable) and one-to-one (injective). In a recent series of papers [12]-[14], Letellier et al. computed the nonlinear

observability matrices for the well-known Lorenz and Rössler systems [15], [16] and demonstrated that the order of the singularities present in the observability matrix (and thus the amount of intersection between the singularities and the phase space trajectories) was related to the decrease in observability.

For a nonlinear system A_{NL} in the form (1), the scalar measurement function is taken as $y(t) = C\mathbf{x}$ and the system equations comprise the nonlinear vector field $\mathbf{f}(\mathbf{x}) = A_{NL}\mathbf{x}$ (note: if there is no external input, then $B\mathbf{u} = 0$). Differentiating $y(t)$:

$$\dot{y}(t) = \frac{d}{dt}C\mathbf{x} = \frac{dC}{dt}\dot{\mathbf{x}} = \frac{dC}{dt}A_{NL}\mathbf{x} = L_f y(\mathbf{x}) \quad (3)$$

where $L_f y(\mathbf{x})$ is the Lie derivative of y along the vector field \mathbf{f} . The differential embedding map ϕ is defined as the Lie derivatives $L_f^0 y(\mathbf{x}) \dots L_f^{n-1} y(\mathbf{x})$, and taking the Jacobian of the map we arrive at the observability matrix:

$$O = \frac{\partial \phi}{\partial \mathbf{x}} = \begin{bmatrix} \frac{\partial L_f^0 y(\mathbf{x})}{\partial \mathbf{x}} \\ \frac{\partial L_f^1 y(\mathbf{x})}{\partial \mathbf{x}} \\ \vdots \\ \frac{\partial L_f^{n-1} y(\mathbf{x})}{\partial \mathbf{x}} \end{bmatrix} \quad (4)$$

which reduces to (2) for linear system representations. The key intuition here is that in the nonlinear case the observability matrix becomes a function of the states, where a linear system is always a constant matrix of parameters.

C. Observability Index

In systems with real numbers, calculation of the Kalman rank condition may not yield an accurate measure of the relative closeness to singularity (conditioning) of the observability matrix. It was demonstrated in [4] that the calculation of a matrix condition number [17] would provide a more robust determination of the ill-conditioning inherent in a given observability matrix. The observability index $\delta(\mathbf{x})$ is given in [4], however we will use the inverted form in [18] so that $0 \leq \delta(\mathbf{x}) \leq 1$

$$\delta(\mathbf{x}) = \frac{|\lambda_{\min} [O^T O]|}{|\lambda_{\max} [O^T O]|} \quad (5)$$

where $\delta(\mathbf{x}) = 1$ indicates full observability and $\delta(\mathbf{x}) = 0$ indicates no observability.

III. Observability of 3-node Fitzhugh-Nagumo network motifs

A. Fitzhugh-Nagumo System Dynamics

The Fitzhugh-Nagumo (FN) equations [19], [20], comprise a general representation of an excitable neuronal membrane. The model is used as a 2-dimensional analogue of the well known Hodgkin-Huxley model [21]: an axonal excitable membrane with ionic currents and voltage gated ion channels. The FN model can exhibit a variety of dynamical modes which

include active transients, limit cycles, and chaos [19]. The nonlinear connection function takes the form of the sigmoidal activation function of neighboring activity (hyperbolic tangent) and an exponential decay with inter-nodal distance to convey the connection/coupling strength.

The system dynamics at a node are given by the equations [19]:

$$\begin{aligned}\dot{v} &= c(v - \frac{v^3}{3} + w + f_{NL}(v^*, d) + I) \\ \dot{w} &= \frac{-1}{c}(v - a + bw)\end{aligned}\quad (6)$$

where v represents membrane voltage, w is recovery, d the inter-nodal distance, v^* the voltage of neighbor nodes, $I = -1.15$ the input current, and the standard parameters $a = 0.7$, $b = 0.8$, $c = 3$. In the following analysis, we are interested in directed information flow between nodes as a function of various topological connection motifs. As such, each motif is representative of a unique combination of directed connections in between the 3 nodes. We utilize a hyperbolic tangent in the nonlinear connectivity function:

$$f_{NL}(v^*, d) = \frac{k}{2}(\tanh(\frac{v^* - h}{2w}) + 1)e^{-d}v^* \quad (7)$$

The sigmoid parameters $k = 1$, $h = 0$, $w = 1/4$, are set such that \tanh outputs $[0,1]$ for the input $[-2,2]$, which is the range of the typical FN voltage variable. In this configuration inputs from neighboring nodes act in an excitatory-only manner, while the driving input current $I = -1.15$ was applied to all three nodes and provided a limit cycle regime to the network for certain network connection strengths.

To contrast for the linear case, we piecewise linearize the Heaviside threshold function in the Wilson-Cowan equations [22], thereby removing the nonlinearity and admitting a network with true linear nodal dynamics. The system dynamics at a node are given by the state space [23]:

$$\begin{aligned}\dot{v} &= c_1v + c_2a + c_3e^{-d}H(v^* - c_4) \\ \dot{a} &= c_5v + c_6a\end{aligned}\quad (8)$$

where v represents activity, a is recovery, d the inter-nodal distance, v^* the activity of neighbor nodes, and $H(\cdot)$ the Heaviside function.

B. Network Motifs

As we are interested in the effect of connection topology on observability, we start with the simplest nontrivial network: a 3-node network. These 3-node network motifs are highly overrepresented in both neuronal and other complex system networks [24]. For each network motif shown in Fig. 1, we compute the observability index for various measurement functions, nodal equations, and connection strengths. Measurements of v for each motif were from nodes 1, 2, then 3. Simulated data was used to compute the observability index for two cases: 1) the nodal dynamics comprise the nonlinear Fitzhugh-Nagumo equations, and 2) the nodal dynamics are linear Wilson-Cowan equations [22]. The data comprise 100

seconds of FN system dynamics with a time step of $dt = 0.04$ integrated using the Runge-Kutta 4th order (RK4) method. These calculations are summarized in the Fig.1 for the observability for the various network motifs.

C. Construction of the Differential Embedding Map

As an example case we begin constructing the observability matrix for motif 1 (shown in Fig.1), the FN network equations form the nonlinear vector field \mathbf{f} :

$$\mathbf{f} \begin{cases} f1=c(v_1 - \frac{v_1^3}{3} + w_1 + f_{NL}(v_2, v_3, d_{12}, d_{13})) \\ f2=\frac{-1}{c}(v_1 - a + bw_1) \\ f3=c(v_2 - \frac{v_2^3}{3} + w_2 + f_{NL}(v_1, v_3, d_{21}, d_{23})) \\ f4=\frac{-1}{c}(v_2 - a + bw_2) \\ f5=c(v_3 - \frac{v_3^3}{3} + w_3 + f_{NL}(v_1, v_2, d_{31}, d_{32})) \\ f6=\frac{-1}{c}(v_3 - a + bw_3) \end{cases} \quad (9)$$

and the measurement function for node 1 in motif 1 is $y = \mathbf{C}\mathbf{x} = [1, 0, 0, 0, 0, 0]\mathbf{x} = v_1$.

Construct the differential embedding map by taking the Lie derivatives from $L_f^0 y(\mathbf{x}) = v_1$ to $L_f^{n-1} y(\mathbf{x})$ shown in (10).

$$\phi \begin{cases} y=v_1 \\ f1=c(v_1 - \frac{v_1^3}{3} + w_1 + f_{NL}(v_2, v_3, d_{12}, d_{13})) \\ \frac{\partial \phi_2}{\partial v_1} f1 + \frac{\partial \phi_2}{\partial w_1} f2 + \frac{\partial \phi_2}{\partial v_2} f3 + \frac{\partial \phi_2}{\partial w_2} f4 + \frac{\partial \phi_2}{\partial v_3} f5 + \frac{\partial \phi_2}{\partial w_3} f6 \\ \frac{\partial \phi_3}{\partial v_1} f1 + \frac{\partial \phi_3}{\partial w_1} f2 + \frac{\partial \phi_3}{\partial v_2} f3 + \frac{\partial \phi_3}{\partial w_2} f4 + \frac{\partial \phi_3}{\partial v_3} f5 + \frac{\partial \phi_3}{\partial w_3} f6 \\ \frac{\partial \phi_4}{\partial v_1} f1 + \frac{\partial \phi_4}{\partial w_1} f2 + \frac{\partial \phi_4}{\partial v_2} f3 + \frac{\partial \phi_4}{\partial w_2} f4 + \frac{\partial \phi_4}{\partial v_3} f5 + \frac{\partial \phi_4}{\partial w_3} f6 \\ \frac{\partial \phi_5}{\partial v_1} f1 + \frac{\partial \phi_5}{\partial w_1} f2 + \frac{\partial \phi_5}{\partial v_2} f3 + \frac{\partial \phi_5}{\partial w_2} f4 + \frac{\partial \phi_5}{\partial v_3} f5 + \frac{\partial \phi_5}{\partial w_3} f6 \end{cases} \quad (10)$$

We obtain the observability matrix by taking the Jacobian of (10). In this FN network the observability matrix is dependent on the state variables and thus a function of the location in phase space. In this situation, Letellier et al. [12] used averages of the observability index over the state trajectories in phase space as a qualitative measure of observability. We also adopt this convention in the results section when computing observability of various network motifs. The indices are computed for each time point in the trajectory, then the average is computed over all of the time points.

IV. Results

For motif 1 (Fig.1), the data (in black) show that a symmetry caused by the connection topology and identical nodal parameters generate very low observability indices. The values are averaged over a few system trajectories and the measurements from each node yield nearly identical values as we expect them to be for a symmetric system. This is further evidenced by the several orders of magnitude decrease in the indices for the linear calculation (in red), where the symmetry creates fixed singularities in the reconstruction map. In motif 2, observability is confounded when a reconstruction map is created from measurements of node 2, as the inputs from nodes 1 and 3 become ambiguous and distinguishability is lost. In the cases where the indices are zero (motifs 4,5, and 7), the motif

must contain an isolated or immeasurable node(s). From the viewpoint of observability this means that information from the ‘isolated’ node(s) cannot reach the measured node. This nodal ‘isolation’ is exemplified in motif 7 and fits well with the theory of Structural Controllability and Observability from Lin [25] and Rech and Perret [26].

In Fig.2, data points are shown for averaged observability indices for the nonlinear FN network in motif 2. These data are averaged over a time course of 2400 timesteps for each simulated trajectory for a different network connection strength value, as measured from each node. The results show the synchrony of nodes 1 and 3, demonstrated in Fig.3, confounds the reconstruction when measured from node 2. The observability is higher for stronger coupling strengths when measuring from nodes 1 or 3 as compared to measuring from node 2 where symmetry creates ambiguity (singularities) in the reconstruction. This phenomenon is more clearly visualized in Fig.4, where locations in phase space with high observability are marked with an asterisk on the trajectories passing through these regions. The nonlinearities in a network cause observability to become a function of the state variables. The dynamics in these systems can move near the singularities present in the particular reconstruction map created from a single time series measurement function which causes poor observability. As our results demonstrate here, the observability is not only influenced by the nodal dynamics, but also by the strength and configuration of the network connections.

V. Discussion

The effects of network topology, connection strength, nonlinearities, and symmetry on the effective observability were evaluated for Fitzhugh-Nagumo (nonlinear) and Wilson-Cowan (linear) neuronal networks. To our knowledge, this is the first quantification of dynamical observability in networked biological models of neuronal activity.

In certain cases of topologic symmetry (motif 1, motif 2 measured from node 2) the identical nodal parameters cause the system to become unobservable in the linear case and nearly unobservable in the nonlinear case. These results agree with the views of symmetries presented in [13], which underscores the importance of careful model selection and measurement when reconstructing dynamics from data. Observation in motif 3 seems to suggest a relationship between the degree of connections into and out of a node and its effective observability. A more complete exploration of the relation of network structure to observability in the nonlinear context is clearly warranted.

Acknowledgments

Supported by grants from the National Academies - Keck Futures Initiative, and Collaborative Research in Computational Neuroscience NIH grant IROIEBOI4641.

References

1. Schiff, SJ. *Neural Control Engineering*. MIT Press; Cambridge: 2012.
2. Voss H, Timmer J, Kurths J. Nonlinear dynamical system identification from uncertain and indirect measurements. *International Journal of Bifurcation and Chaos*. 2004; 14:1905–1933.

3. Sauer TD, Schiff SJ. Data assimilation for heterogeneous networks: The consensus set. *Phys Rev E*. 2009; 79:051909.
4. Friedland B. Controllability index based on conditioning issue. *Journal of Dynamic Systems, Measurement, and Control*. 1975; 97:444.
5. Kalman R. Mathematical description of linear dynamical systems. *SIAM Journal on Control*. 1963; 1:152–192.
6. Kailath, T. *Linear Systems*. Prentice-Hall; Upper Saddle River: 1980.
7. Hermann R, Krener A. Nonlinear controllability and observability. *Automatic Control, IEEE Transactions on*. 1977; 22:728–740.
8. Haynes G, Hermes H. Nonlinear controllability via Lie theory. *SIAM Journal on Control*. 1970; 8:450–460.
9. Whitney H. Differentiable manifolds. *The Annals of Mathematics*. 1936; 37:645–680.
10. Takens F. Detecting strange attractors in turbulence. *Lecture Notes in Mathematics*. 1981:366–381.
11. Sauer T, Yorke Ja, Casdagli M. Embedology. *Journal of Statistical Physics*. 1991; 65:579–616.
12. Letellier C, Maquet J, Sceller L, Gouesbet G, Aguirre L. On the non-equivalence of observables in phase-space reconstructions from recorded time series. *Journal of Physics A: Mathematical and General*. 1998; 31:7913–7927.
13. Letellier C, Aguirre La. Investigating nonlinear dynamics from time series: The influence of symmetries and the choice of observables. *Chaos*. 2002; 12:549–558. [PubMed: 12779585]
14. Letellier C, Aguirre L, Maquet J. Relation between observability and differential embeddings for nonlinear dynamics. *Physical Review E*. 2005; 71:1–8.
15. Lorenz E. Deterministic nonperiodic flow. *Journal of the atmospheric sciences*. 1963; 20:130–141.
16. Rössler O. An equation for continuous chaos. *Physics Letters A*. 1976; 57:397–398.
17. Strang, G. *Linear Algebra and Its Applications*. 4. Brooks Cole; St. Paul: 2005.
18. Aguirre L. Controllability and observability of linear systems: some noninvariant aspects. *IEEE Transactions on Education*. 1995; 38:33–39.
19. Fitzhugh R. Impulses and Physiological States in Theoretical Models of Nerve Membrane. *Biophysical Journal*. 1961; 1:445–466. [PubMed: 19431309]
20. Nagumo J, Arimoto S, Yoshizawa S. An active pulse transmission line simulating nerve axon. *Proceedings of the IRE*. 1962; 50:2061–2070.
21. Hodgkin AL, Huxley AF. A quantitative description of membrane current and its application to conduction and excitation in nerve. *J Physiol*. 1952; 117:500. [PubMed: 12991237]
22. Wilson HR, Cowan JD. A mathematical theory of the functional dynamics of cortical and thalamic nervous tissue. *Kybernetik*. 1973; 13:55–80. [PubMed: 4767470]
23. Pinto DJ, Ermentrout GB. Spatially Structured Activity in Synaptically Coupled Neuronal Networks: I. Traveling Fronts and Pulses. *SIAM Journal on Applied Mathematics*. 2001; 62:206–225.
24. Milo R, Shen-Orr S, Itzkovitz S, Kashtan N, Chklovskii D, Alon U. Network motifs: simple building blocks of complex networks. *Science*. 2002; 298:824–7. [PubMed: 12399590]
25. Lin C-T. Structural controllability. *Automatic Control, IEEE Transactions on*. 1974; 19:201–208.
26. Rech C, Perret R. Structural observability of interconnected systems. *International Journal of Systems Science*. 1990; 21:1881–1888.

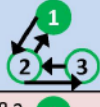
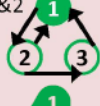
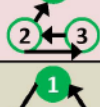
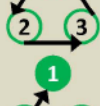
| Network Motif : | Measure Node 1 | Measure Node 2 | Measure Node 3 | Symmetry | |
|---|--|---|---|---|----------------|
| Valance 2 1)  | $\delta_{NL}(x) = 1.5 \times 10^{-11}$ $\delta < 10^{-16}$ | $\delta_{NL}(x) = 2.9 \times 10^{-11}$ $\delta < 10^{-16}$ | $\delta_{NL}(x) = 1.5 \times 10^{-11}$ $\delta < 10^{-16}$ | S_3 | |
| | 2)  | $\delta_{NL}(x) = 9.0 \times 10^{-11}$ $\delta = 9.2 \times 10^{-6}$ | $\delta_{NL}(x) = 1.6 \times 10^{-11}$ $\delta < 10^{-16}$ | $\delta_{NL}(x) = 8.8 \times 10^{-11}$ $\delta = 9.2 \times 10^{-6}$ | [123] [321] |
| Valance 1&2 3)  | $\delta_{NL}(x) = 6.9 \times 10^{-10}$ $\delta = 4.2 \times 10^{-6}$ | $\delta_{NL}(x) = 2.4 \times 10^{-10}$ $\delta = 8.5 \times 10^{-6}$ | $\delta_{NL}(x) = 2.2 \times 10^{-11}$ $\delta = 8.8 \times 10^{-6}$ | [123] | |
| | 4)  | $\delta_{NL}(x) = 4.5 \times 10^{-12}$ $\delta = 8.5 \times 10^{-6}$ | $\delta_{NL}(x) = 7.0 \times 10^{-11}$ $\delta < 10^{-16}$ | $\delta_{NL}(x) = 0$ $\delta = 0$ | [123] |
| | 5)  | $\delta_{NL}(x) = 1.1 \times 10^{-10}$ $\delta = 8.8 \times 10^{-6}$ | $\delta_{NL}(x) = 0$ $\delta = 0$ | $\delta_{NL}(x) = 0$ $\delta = 0$ | [123] |
| Valance 1 6)  | $\delta_{NL}(x) = 8.8 \times 10^{-11}$ $\delta = 8.1 \times 10^{-6}$ | $\delta_{NL}(x) = 1.0 \times 10^{-10}$ $\delta = 8.1 \times 10^{-6}$ | $\delta_{NL}(x) = 9.2 \times 10^{-11}$ $\delta = 8.1 \times 10^{-6}$ | [123] [231] [312] | |
| | 7)  | $\delta_{NL}(x) = 2.7 \times 10^{-12}$ $\delta = 8.1 \times 10^{-6}$ | $\delta_{NL}(x) = 0$ $\delta = 0$ | $\delta_{NL}(x) = 0$ $\delta = 0$ | [123] |

Fig. 1. Calculation of observability indices for each of the 7 network motifs, as measured from each node and averaged over a range of network connection strengths. In black, the observability indices represent the computations for nonlinear Fitzhugh-Nagumo networks, while in red are for linear Wilson-Cowan networks. The calculations show the effect of network topology, nonlinearities, and choice of measurement function on observability.

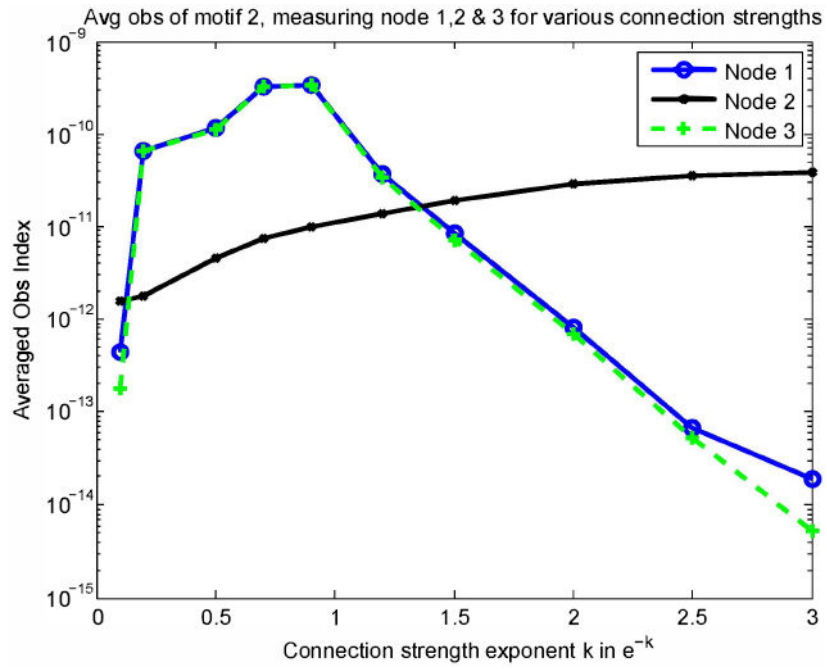


Fig. 2.

Trends of averaged observability as a function of connection strength, plotted for each node in motif 2. As connection strength decreases from left to right, the average observability changes for each node in motif 2, showing the effects of symmetry as measuring from nodes 1 and 3 is more observable at stronger coupling than measuring from node 2 (the symmetric case)

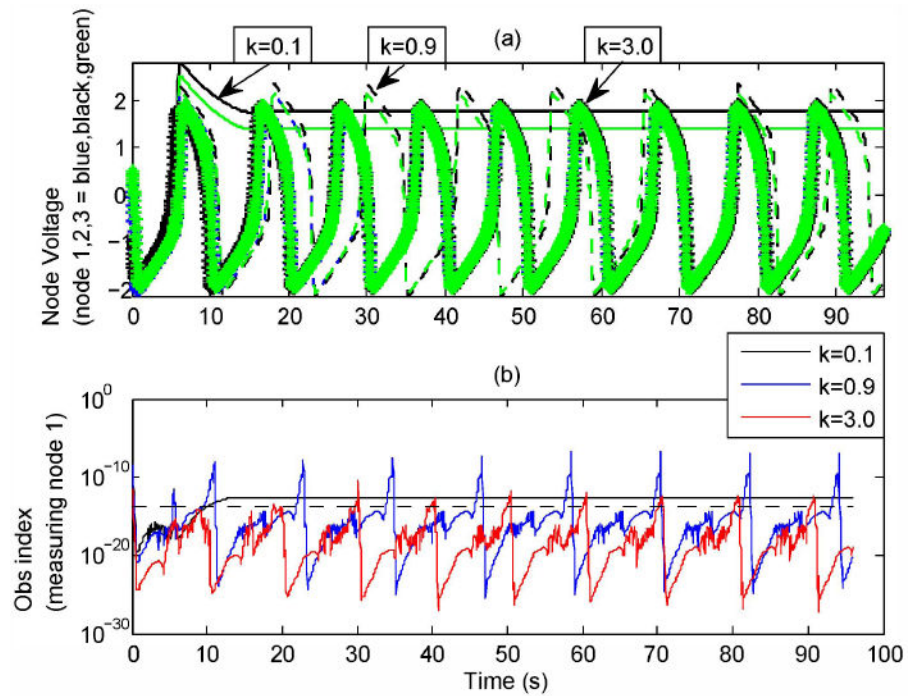


Fig. 3.

(a) The 3-node dynamics for a FN network of motif 2, showing trajectories for a range of connection strengths. Here the decrease in nodal connection strength facilitates faster firing, and the network symmetry present in motif 2 causes the dynamics of nodes 1 and 3 to synchronize despite differences in initial conditions. (b) The local network observability index measured from node 1 for motif 2. The black dashed line is the average observability index value for motif 2 as measured from node 1. This average value is used as a threshold for the points of local observability above the mean value in Fig.4

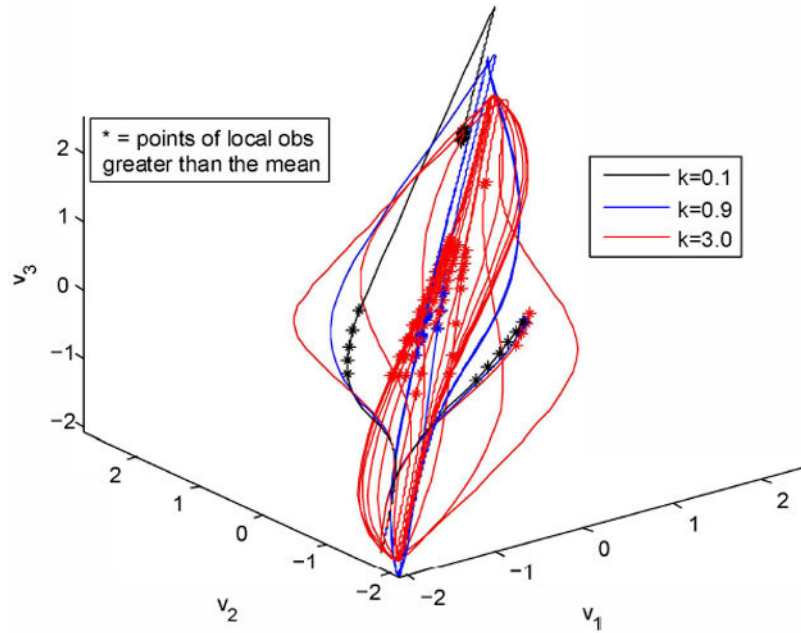


Fig. 4.

The 3-dimensional phase space for v , showing trajectories in motif 2 for a range of connection strengths. The connection strengths that are on average more observable visit regions of phase space that are observable more frequently, which in the FN system case is a portion of the trajectories contained in a limit cycle. Connectivities that cause faster (limit cycle) firing lead to more observability (averaged over time).